Journal of Power Sources 248 (2014) 915–922

Contents lists available at ScienceDirect

Journal of Power Sources

journal homepage: www.elsevier.com/locate/jpowsour

Performance of $LiNi_{1/3}Mn_{1/3}Co_{1/3}O_2$/graphite batteries based on aqueous binder

Nicholas Loeffler, Jan von Zamory, Nina Laszczynski, Italo Doberdo, Guk-Tae Kim*, Stefano Passerini*

Institute of Physical Chemistry & MEET Battery Research Centre, University of Muenster, Germany

HIGHLIGHTS

- Manufacturing of CMC-based electrodes for Li-ion batteries.
- Successful aqueous processing of water-sensible NMC cathode material.
- Thermal and electrochemical stability of CMC binder.
- Effect of calendering on CMC-based electrodes.
- Superior long-term cycling performance of CMC-based Li-ion cells.

ARTICLE INFO

Article history:
Received 6 August 2013
Received in revised form
10 September 2013
Accepted 1 October 2013
Available online 15 October 2013

Keywords:
Aqueous electrode processing
Sodium carboxymethylcellulose
Binder
Lithium-ion batteries
$LiNi_{1/3}Mn_{1/3}Co_{1/3}O_2$ (NMC)
Graphite

ABSTRACT

This manuscript reports on the manufacturing and characterization of sodium carboxymethylcellulose-based, Li-ion positive electrodes with high active material mass loadings using only water as a solvent. The effect of different calendering forces on the aqueous processed cathode electrodes is also reported. Finally, the performance of balanced full Li-ion cells in pouch cell configuration is investigated. These Li-ion cells subjected to long-term cycling experiment displayed an average coulombic efficiency of 99.96% and retained a specific capacity of almost 70% of its initial capacity after 2000 cycles.

1. Introduction

From the electrochemical point of view Li-ion batteries consist of “active” and “inactive” components [1]. At the electrode level, only the cathode and anode active materials are listed among the “active” components whereas the binder, conductive agent and current collector, which do not directly contribute to the electrochemical processes (i.e., to the specific capacity of the battery), are summarized as “inactive” components. Despite the attribute “inactive”, these components may have a quite significant impact on cell performance and can also contribute to reversible and irreversible capacities within the cell [2–4]. In fact, the capacity of an electrode is influenced by the active material mass loading (mg cm^{-2}) and density (mg cm^{-3}). These parameters are determined by the thickness of the coating, density, porosity and the active material content in the slurry [5]. Especially the nature of the binder significantly influences these parameters. This latter component is supposed to hold the electrode’s active material particles in touch with each other and the conductive additive (cohesion) and ensure a superior bonding of the composite electrode to the current collector (adhesion) [6–8]. Moreover, the binder needs to buffer the volume expansions which occur during (de)lithiation of the active material particles [8–10]. For being deployed in a Li-ion battery, the binder should be electrochemically stable in a wide voltage range extending from about 0 V to 5 V vs. Li/Li^+ and chemically resistant to other cell components (electrolyte). Fulfilling most of these requirements,

* Corresponding authors.
E-mail addresses: kimguktae@uni-muenster.de (G.-T. Kim), stefano.passerini@uni-muenster.de (S. Passerini).

0378-7753/$ – see front matter © 2013 Elsevier B.V. All rights reserved.
http://dx.doi.org/10.1016/j.jpowsour.2013.10.018

polyvinylidene-di-fluoride (PVdF) is nowadays the state of the art binder in commercial Li-ion batteries, especially for cathodes [11]. Nevertheless it exhibits a few serious drawbacks. Like all fluorinated polymers, its poor recyclability is problematic with respect to the environment. Furthermore, its use is accompanied by the utilization of the volatile, expensive and highly toxic solvent *N*-methyl-pyrrolidone (NMP). Additionally with a price of around 15–18 EUR kg^{-1}, PVdF is a relatively costly polymer [12,13]. Hence a growing interest is focussing on the substitution of PVdF with environmentally benign binders, which are water soluble. This would result in significant process cost savings and vast reduction of toxic material use, resulting in an environmentally more sustainable way of producing Li-ion batteries [14,15].

There is a growing spectrum of possible water soluble binders for electrode preparation comprising different kinds of binder materials, e.g. rubbers [16,17], gums [18,19], and other polysaccharides [20,21] of which the sodium salt of carboxymethylcellulose (CMC) seems to be the most promising candidate [12,13,22,23]. CMC is cheap (1–2 EUR kg^{-1}), water soluble, easy disposable and has already proven to be an adequate replacement for PVdF concerning the anode (graphite) electrode [14,24,25].

Recent works showed that CMC is also feasible as a binder for different cathode materials [15,23,26,27]. Nevertheless, only few results have been, so far, reported on its use in lithium-ion battery cathodes. To close this gap and further shorten the distance between lab-scale experiments and industrial production, this manuscript is focused on demonstrating a way of manufacturing a CMC-based, lithium-ion cells with high cathode mass loadings, i.e., close to those used in commercial lithium-ion batteries. As lithium nickel–manganese–cobalt dioxide ($LiNi_{1/3}Mn_{1/3}Co_{1/3}O_2$ or NMC) is among the presently used active cathode material [11] for commercial batteries, we decided to combine the NMC cathode with a graphite anode (SLP 30).

2. Experimental

2.1. Electrode processing

Commercially available NMC (Toda, average particle size: $d_{90} = 10$ μm) and SLP 30 graphite (Timcal, average particle size: $d_{90} = 32$ μm) were used as delivered. Sodium carboxymethyl cellulose (CMC, Dow Wolff Cellulosics, Walocel CRT 2000 PPA 12) with a degree of substitution of 1.2 was used as binder, while the conducting agent carbon black was C-NERGY Super C45 (Timcal, primary average particle size: 30 nm). The anode and cathode electrodes were prepared in the following way: CMC was firstly dissolved in deionized water at room temperature by magnetic stirring. After complete solvation of CMC the solution was transferred to a steel vessel and the required amount of Super C45 was added. Further stirring was conducted with a dispersing system (Dispermat VL, VMA GmbH) at medium stirring speed (2000 rpm) for approximately 4 h. The required amount of active material was then added into the aqueous mixture and the slurry was further homogenized at 20 °C for 3 h using the Dispermat dissolver. In a final step the slurry was mixed at lower stirring speed (200 rpm) under vacuum for 10–30 min.

The so-obtained anode slurry was transferred to a pre-pilot automated coating line (Hohsen Corp, Coating Machine HSCM-20802i) and casted on copper foil (thickness: 10 μm). The coated electrode was immediately dried in the heating zone (130 °C) of the coating machine in ambient air.

The obtained cathode slurry was cast on aluminium foil (thickness: 20 μm), which was previously coated with a carbon dispersion (Timcal, C-NERGY Li-Quid 101) to prevent corrosion of the aluminium current collector, by using a laboratory scale blade coater [28]. The coated electrode was immediately pre-dried in an atmospheric oven (Binder, ED-115) at 80 °C for 30 min.

The dried anode and cathode electrodes were cut into stripes of 6 cm width and roll-pressed with a calendering machine (Hohsen Corp, Roll Press Machine HSRP-2025) at different pressures.

Viscosity measurements of all slurries were carried out at shear rates of 100 s^{-1} and 500 s^{-1} using a rheometer (Thermo Scientific, HAAKE Viscotester 550).

The composition of the dried cathode electrode tape was 88 wt.% NMC, 7 wt.% Super C45 and 5 wt.% CMC while that of the anode electrode tape was 90 wt.% SLP 30, 5 wt.% Super C45 and 5 wt.% CMC. The average mass loadings of cathode and anode electrodes were about 7.5 mg cm^{-2} and 3.3 mg cm^{-2}, respectively.

2.2. Cell assembling

For the half-cell tests cathode and anode disc electrodes with an area of 1.13 cm^2 were cut out of the electrode tapes. The electrode discs were dried at 170 °C under vacuum for 12 h.

The cathode half-cells were prepared in pouch bag configuration with metallic lithium (Rockwood Lithium, thickness: 50 μm, battery grade) as counter electrode. Aluminium tabs were used to connect the NMC electrode, while nickel tabs were used for the lithium electrode. A commercially available single layer polyethylene membrane (Asahi Kasei, Hipore SV718) was used as separator. All pouch bag half-cells were assembled in a dry-room (R.H. $< 0.1\%$) at 20 °C ± 1 °C.

The anode half-cells were prepared in the three-electrode Swagelok cell system with metallic lithium (Rockwood Lithium, battery grade) as counter and reference electrode. A glass fibre separator (Whatman, GF/D) drenched in electrolyte was used for the Swagelok cells, which were assembled in an argon filled glove box (MBraun, Labmaster DP) with oxygen and water contents lower than 1 ppm.

Lithium-ion full cells were also assembled in the pouch bag configuration. The cathode and anode electrodes with an active area of, respectively, 16 cm^2 and 19.36 cm^2 were cut out of the electrode tapes and dried at 170 °C under vacuum for 12 h. Nickel (anode) and aluminium (cathode) tabs were used as cell terminals. Asahi separator was used in the full cells, which were assembled in the dry-room by piling up anode, separator and cathode. For all the assembled cells the commercial electrolyte consisting of 1 mol L^{-1} $LiPF_6$ EC:DMC 1:1 w/w (Merck AG, LP 30) was used.

2.3. Electrode characterization

All electrochemical tests were performed with a Maccor Battery tester 4300 at room temperature (20 °C ± 2 °C). The cathode half-cell tests were carried out between 3.0 V and 4.3 V vs. Li/Li^+ with an initial charge/discharge rate of 0.1 C for 3 cycles followed by a constant cycling at 1 C rate. The cycling tests of all cathode electrodes were performed in galvanostatic conditions (CC). The anode half-cell tests were carried out between 0.02 V and 1.50 V vs. Li/Li^+ with an initial charge/discharge rate of 0.1 C for 6 cycles. Further cycling was performed at 1C rate for 20 cycles, then increased to 2 C rate for additional 20 cycles and finally followed by a constant cyclization at 1 C rate. All anode tests were performed as galvanostatic and potentiostatic measurements (CCCV). The full-cell measurements were also carried out with CCCV tests in a voltage range between 2.75 V and 4.20 V.

Scanning electron microscopy (SEM) imaging of the different pressed electrodes was performed using a Zeiss EVO MA 10 microscope.

2.4. Binding agent characterization

2.4.1. Thermal gravimetric analysis (TGA)

Thermogravimetric measurements of the pure CMC powder were performed with a Q 5000 IR TGA instrument (TA Instruments). Platinum pans filled with 15–25 mg of sample were heated from room temperature to 1000 °C with a heating rate of 10 °C min^{-1}, using nitrogen (25 mL min^{-1}) or oxygen (25 mL min^{-1}) as purge gas.

2.4.2. Cyclic Voltammetry (CV)

Cyclic Voltammetry (CV) investigations of the pure CMC binder were carried out using a VMP3 (BioLogic). Therefore the CMC was dissolved in deionized water, casted on aluminium or copper foils with a lab scale blade coater and immediately pre-dried in an atmospheric oven at 80 °C for 30 min. Electrodes with an area of 1.13 cm^2 were cut out of the CMC-coated metal foils and dried at 140 °C under vacuum for 12 h. The CV measurements were performed in Swagelok cells with the same set-up as the previously described anode half-cells (see 2.2). The tests were carried out at a scan rate of 0.5 mV s^{-1} and a scan range for the CMC-coated aluminium and copper foil of, respectively, 1.5 V–5 V and 0.02 V–2.50 V.

3. Results and discussion

3.1. Binder stability

The performance of a Li-ion battery is strongly affected by the electrochemical and thermal stabilities of the CMC binder used to make the composite electrodes. To verify the binder thermal stability TGA measurements in oxygen and nitrogen were performed on CMC powder. The thermogravimetric measurements of CMC binder in oxygen as well as nitrogen atmosphere are shown in Fig. 1a and b. As displayed in Fig. 1a CMC binder is thermally stable in oxygen atmosphere up to 200 °C. At temperatures above 200 °C the material shows a sharp decrease in weight due to the thermal decomposition of the carboxy groups and, finally, the glucopyranose units that make up the cellulose backbone. Above 260 °C approximately 20 wt% residue is left most likely due to the formation of sodium containing ashes. Fig. 1b illustrates the thermal stability of pure CMC powder in the nitrogen atmosphere. It is evident that CMC binder is also stable up to 200 °C in inert gas. Above 230 °C the CMC starts to decompose in several stages until at approximately 800 °C once more the stable sodium residues are obtained [29,30]. Summarizing these data, it can be concluded that the CMC binder is not affected by thermal treatments below 200 °C in air, thus confirming that the electrodes can be pre-dried in air at 130 °C and, finally, under vacuum at 170 °C (see section 2.2 for the electrode drying procedure).

Apart from the thermal stability during the electrode processing, the electrochemical stability of CMC binder during charge/discharge process is also of major importance. Fig. 2a and c show the results of the characterization performed on bare and CMC coated (approx. coating thickness: 1 μm) copper (Fig. 2a and b) and aluminium foils (Fig. 2c and d).

To investigate the electrochemical cathodic stability of the CMC binder, cyclic voltammetry measurements on bare and CMC coated copper foils (some selected cycles are reported in Fig. 2a and b, respectively) were performed in the potential range extending from 0.2 V to 3.0 V vs. Li/Li^+. The results of the CV measurements reveal no evidence of any peak related to increased current flows due to the CMC binder decomposition. Actually, the CMC coating is seen to reduce the cathodic current flowing in the first sweep. Hence the CMC binder is electrochemically stable in-between the potentials occurring at the anode. The peaks appearing during the first cycle of the CV measurement may be attributed to oxygen at 1.7 V and water contamination at 1.1 V. At lower potentials (0.02 V–1.00 V) reduction peaks of solvent components as well as salt anions appeared. The major peak at about 0.6 V, however, is associated to the insertion of lithium in the native copper oxide layer [31,32].

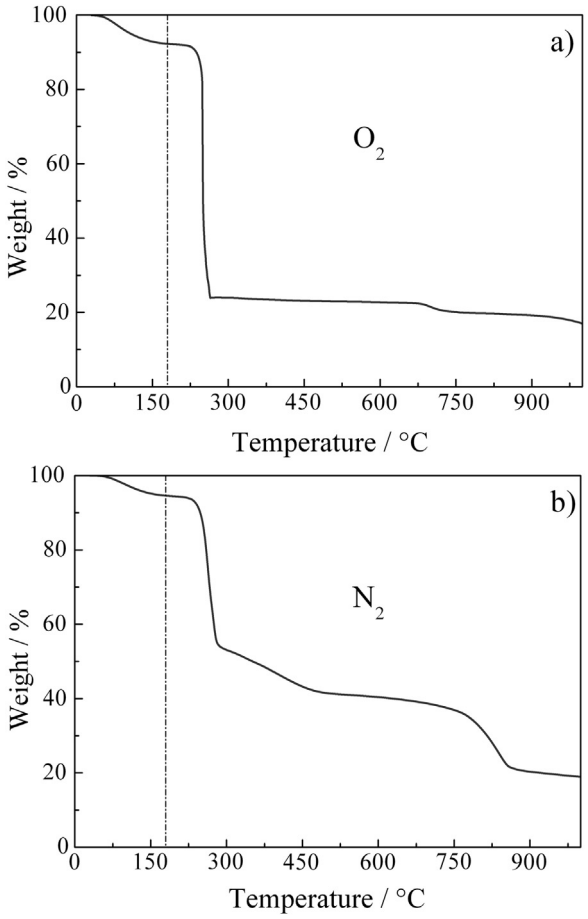

Fig. 1. TGA weight loss profile of CMC powder in oxygen (a) and nitrogen (b) atmospheres.

Fig. 2c displays the CV measurement of aluminium foil. Upon cycling the current response show the expected decrease at high potential (above 4 V vs. Li/Li^+). This stems from the growth of an insulating passivation layer consisting mostly of aluminium fluoride (AlF_3) on the aluminium foil due to electrolyte decomposition, which is protecting aluminium from anodic corrosion [33,34]. This effect is less pronounced for the CMC-coated aluminium foil (Fig. 2d). Considering the narrow current range (between 7 μA and −7 μA) shown in Fig. 2c and d as well as the smooth curve shapes, the CMC binder proofs also to be stable at the potentials occurring at the cathode electrode.

3.2. Anode electrodes

Controlling the slurry viscosity is an important factor which significantly influences the processing and, even, the electrochemical properties of the electrodes [19,24,35]. Especially when increasing the total amount of processed slurry, changing the mixing procedure from lab-scale magnetic stirring to a pre-pilot dissolver (Dispermat), and utilizing a pre-pilot automated coating line for the coating process, monitoring the viscosity is

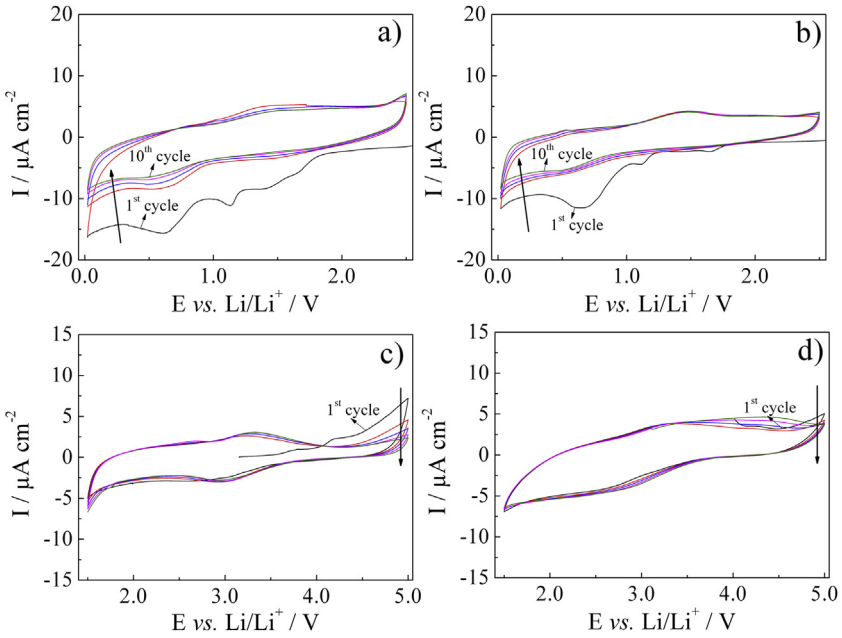

Fig. 2. Selected cyclic voltammograms (1st, 2nd, 3rd, 5th, 10th cycle) of cells with (a) pure Cu foil, (b) CMC coated Cu foil, (c) pure Al foil and (d) CMC coated Al foil working electrodes. Counter and reference electrodes: Li.

indispensable to ensure consistent electrode properties. The anode slurry composition showed a dynamic viscosity of 2.82 Pa s at a shear rate of 100 s^{-1} and 1.03 Pa s at a shear rate of 500 s^{-1} before the coating process. Since the measured viscosity of the electrode dispersion originates primarily from the CMC solution, the viscosity measurement exhibits an expected shear-thinning rheological behaviour. Preinvestigations (data not shown here) revealed that also anode slurries with a two times lower viscosity showed a good processability. Hence, there seems to be a broad viscosity range for processing the anode slurry on the pre-pilot automated coating line. To investigate the cycling performance of anode half-cells upon pressure, the manufactured anode electrodes were roll-pressed at different line force loads (kg cm^{-1}) [36]. However, since graphite materials are sensitive to high calendering forces, the electrodes were subjected only to moderate compression (up to 7 kg cm^{-1}). Table 1 reports the electrode density of the compressed electrodes as well as their thickness reduction (in % of the original thickness).

To verify the effect of electrode calendering, which might endanger the electrode breaking the soft graphite particles and thereby close the electrode pores, SEM characterization was performed. In Fig. 3 are compared the SEM images of un-pressed (Fig. 3a), mildly pressed (3 kg cm^{-1}, Fig. 3b), and heavily pressed (>5 kg cm^{-1}, Fig. 3c) electrodes. As shown by the SEM images no significant differences are visible between the un-pressed and the mildly pressed electrodes. Both electrodes exhibit a homogenous distribution of active material particles and the pores are evenly spread throughout the electrode surface. However, the heavily pressed electrode (Fig. 3c) shows a very flat surface with most of the porosity occluded.

Table 1
Density and thickness reduction of anode electrodes calendered at different pressures.

Calendering force (kg cm^{-1})	Electrode density (g cm^{-3})	Thickness reduction (%)
0	0.77	0
3	0.84	4
5	0.93	11
7	0.99	18

Fig. 4a displays the cycling performance of differently pressed anodes (in half-cell configuration) at current densities corresponding to 1 C and 2 C rate using the CCCV testing mode. The test cells were pre-activated with 6 cycles at 0.1 C rate and for 9 cycles at a 1 C rate to favour the formation of a stable SEI at the interface.

During the first 10 cycles at 1 C rate the delivered capacity of all half-cells continuously increased upon cycling. This can be attributed to a still not optimized electrolyte wetting of the electrode at initial cycling and is maximized in the heavily pressed electrode [12]. However, it becomes apparent that the cycling of the un-pressed electrode performs as well as that of the mildly pressed (3.0 kg cm^{-1}) electrode. The heavily pressed electrodes (5.0 kg cm^{-1} and 7.0 kg cm^{-1}), however, showed a somewhat less stable cycling performance with increasing current density to 2 C and a slightly higher capacity fading after the 50th cycle. Nevertheless, after the 15th cycle the specific capacity varied between 371 mAh g^{-1} and 376 mAh g^{-1} for all of the half-cells. Considering the theoretical specific capacity of SLP 30 to be 372 mAh g^{-1}, these results are quite satisfying. The capacity exceeding the theoretical value obviously originates from the added carbonaceous conductive agent Super C45 [37,38].

Fig. 4b illustrates the voltage profile of the 3 kg cm^{-1} pressed electrode. At the 5th cycle at a current density corresponding to 0.1 C rate, the well-known stages for lithium-ion intercalation in graphite are apparent [39,40]. When increasing the C-rate the intercalation stages are continuously shifted towards lower potentials vs. Li/Li^+. Remarkably the curves of the 25th cycle (before 2 C rate) and the 65th cycle (after 2 C rate) are practically overlapping. The analysis of the depicted voltage profiles supports the results of the morphological investigations and the cycling experiments. On the one hand, the electrochemical behaviour is not negatively influenced by mildly pressing the anode electrodes. On the other hand, highly reversible cycling and an excellent capacity retention, even when increasing to 2 C rate for twenty cycles, is achieved as confirmed by the reproducibility of the voltage profiles.

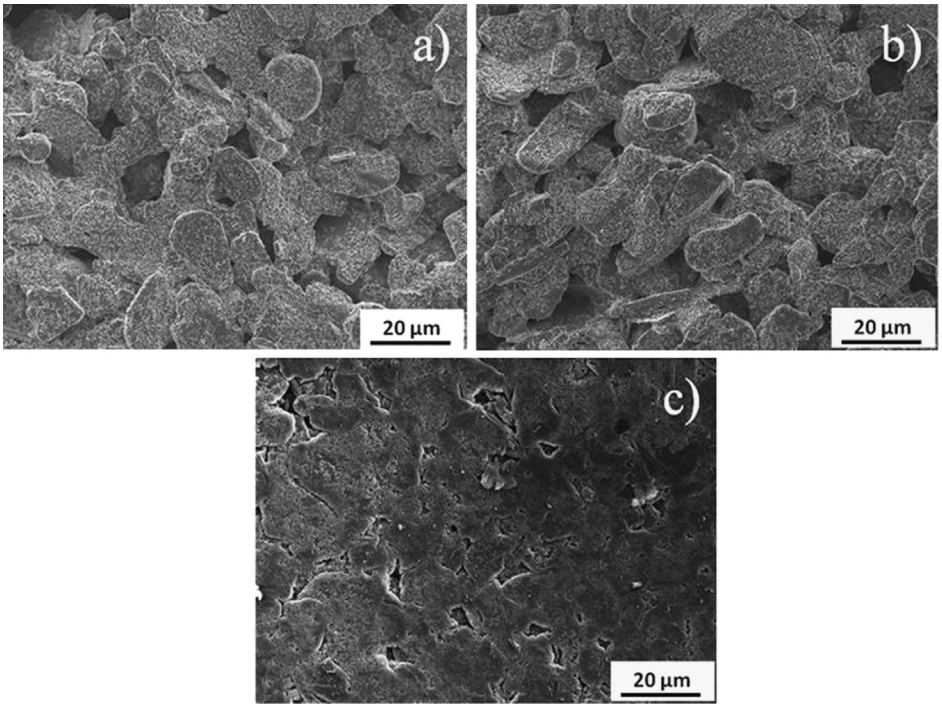

Fig. 3. SEM images of (a) as coated and (b and c) calendered at 3 kg cm^{-1} and >5 kg cm^{-1} SLP 30 anode electrodes.

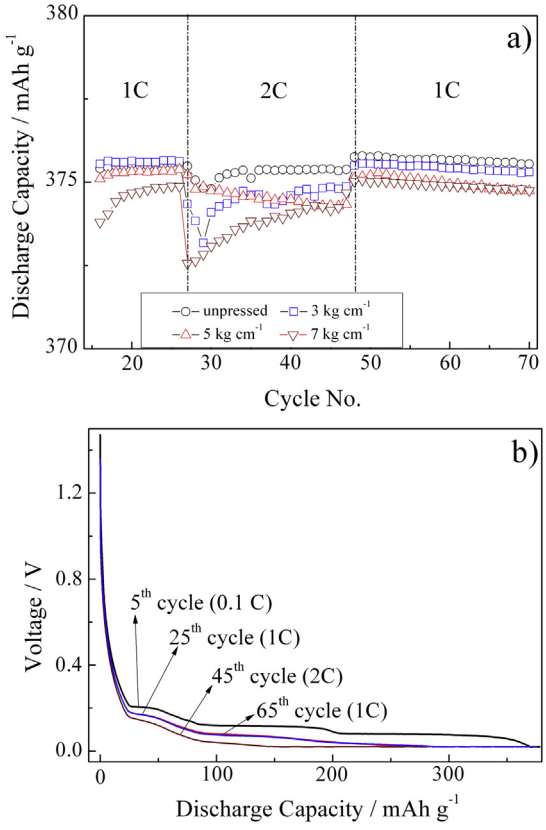

Fig. 4. Cycling performance (a) of SLP 30 anode electrodes pressed with different line force loads and selected voltage profiles (b) of the calendered (line force load: 3 kg cm^{-1}) anode electrode. Counter and reference electrodes: Li.

Overall, considering that the 3 kg cm^{-1} pressed electrode shows very stable cycling behaviour, comparable with that of un-pressed electrodes, as well as a more homogenous growing of the solid electrolyte interface on a flattened electrode surface (and therefore a beneficial effect on the cycling behaviour in a full cell). Hence, the mildly calendered electrode was selected to prepare the lithium-ion batteries [41].

3.3. Cathode electrode

In contrast to the described anode electrode, the aqueous processing of the cathode material is facing an additional challenge: as soon as the NMC material gets into contact with water the pH of the suspension rises up to approximately 11 [42]. Since aluminium, which is standardly used as current collector for the cathode electrode, is chemically not stable at this high pH value, coating of the aqueous NMC slurry results in a serious aluminium corrosion [28]. The substrate degradation is obviously enhanced by the application of thick coatings (here the wet coating thickness was 220 µm) to achieve high electrode mass loading, which results in a large volume of the corrosive fluid on the aluminium foil. The SEM images in Fig. 5a and b show the appearance of an aluminium foil previously coated with the aqueous NMC slurry, which was dried in an atmospheric oven at 80 °C (the NMC coating was removed prior to SEM characterization). Consistently with the results from Ishii et al. [42] and Doberdo et al. [28], the entire surface of the aluminium foil is covered with corrosion products (Fig. 5a). Some distinct corrosion pits (Fig. 5b) perforating the aluminium foil were also observed.

To avoid the corrosion issue and, as a consequence, the capacity losses due to formation of insulating corrosion products and damages to the aluminium current collector [28], two ways of corrosion prevention seem to be viable: First, the addition of a mild acid to the slurry prior to the coating step which results in a lower pH value and therefore prevent the aluminium foil from being corroded. Kim et al. reported that formic acid was used to hinder

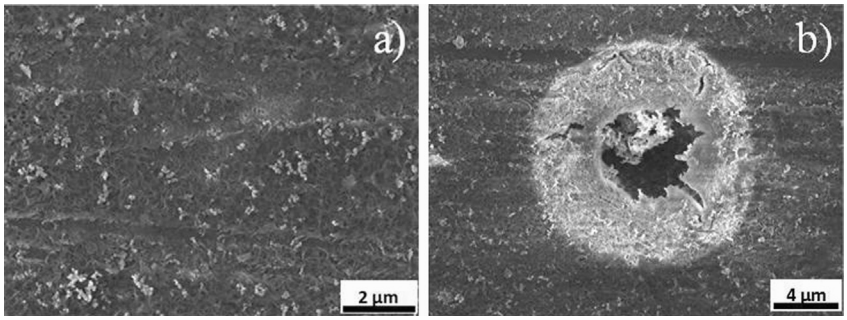

Fig. 5. SEM images of the (a) corroded Al foil surface and (b) of an individual pitting corrosion hole.

Table 2
Concentration of extracted transition metal ions from 2.64 g NMC in 7 mL distilled H_2O at different amounts of formic acid.

Concentration of extracted ions (mg mL^{-1})	Amount of formic acid (mg)				
	0	45	100	180	380
Cobalt	0	0.43	1.20	1.90	4.28
Nickel	0	0.43	1.18	1.85	4.10
Manganese	0	0.48	1.53	2.03	2.13

aluminium corrosion during the manufacturing of aqueous processed $Li_4Ti_5O_{12}$ anode electrodes [12]. Second, a thin carbon layer can be coated on top of the aluminium foil which protects the Al foil from the corrosive aqueous medium [28].

Adding formic acid to slurries comprising NMC as the active material involves the danger of active material damaging due to leaching of transition metal ions. Table 2 reports the metal concentration obtained by ICP analysis of a formic acid–water solution in contact with NMC. Thus, the second approach, apply a carbon coating layer to protect the aluminium foil (see: 2.1) was selected. Since the pre-coating of such a layer was technically difficult to prepare at the used pre-pilot automated coating line, the coating process was carried out at a lab-scale blade coater.

In order to achieve high mass loadings of the cathode electrode the viscosity of the cathode slurry has to be controlled very carefully. The need for sufficiently high cathode mass loadings arises from the need of properly balancing the electrode capacity in the full cells (described later). Because the specific theoretical capacity of the anode active material (372 mAh g^{-1}) exceeds the specific theoretical capacity of the cathode active material (161 mAh g^{-1}) by a factor of nearly two, a cathode with a high active material mass loading is needed for a proper balancing. To achieve high mass loadings of the cathode electrodes, an electrode slurry composition with a dynamic viscosity of 2.31 Pa s at a shear rate of 100 s^{-1} and 0.98 Pa s at a shear rate of 500 s^{-1} was prepared. Naturally the cathode electrode slurry exhibited the same shear-thinning rheological behaviour as the anode electrode one. Adjusting the viscosity to lower values resulted in insufficient mass loadings of the cathode electrode. Adjusting the viscosity to higher values led to an inhomogeneous mixing of the electrode components. Apparently, changes in viscosity seem to have a significantly larger influence on the processability of the cathode slurry compared to the anode one.

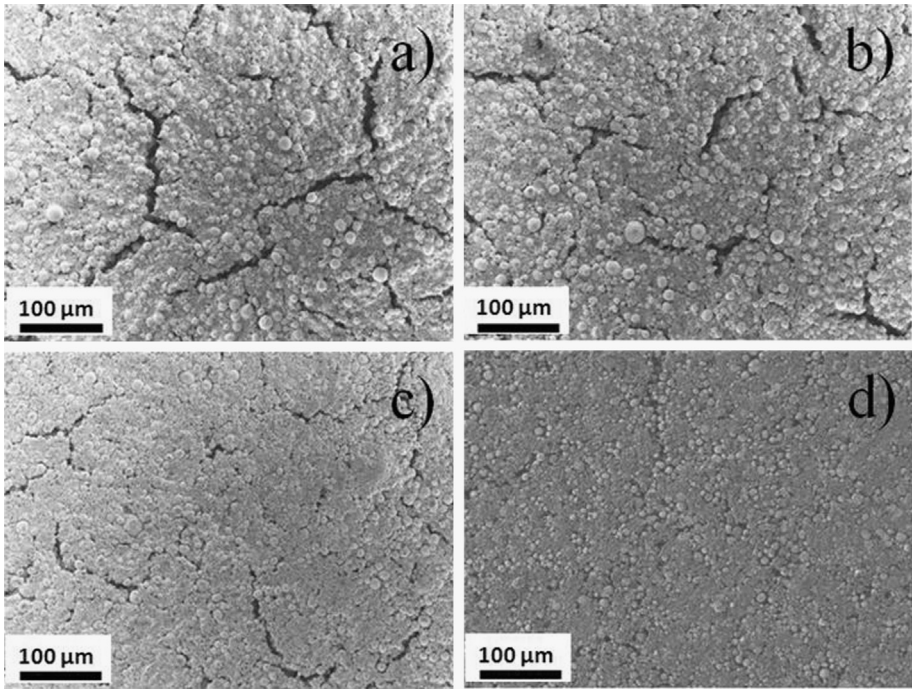

Fig. 6. SEM images of the (a) as coated and calendered NMC cathode electrodes at line force loads of (b) 17 kg cm^{-1}, (c) 47 kg cm^{-1} and (d) 70 kg cm^{-1}.

Table 3
Density and thickness reduction of cathode electrodes calendered at different pressures.

Calendering force (kg cm^{-1})	Electrode density (g cm^{-3})	Thickness reduction (%)
0	1.49	0
17	1.57	13
40	1.66	18
70	1.88	28

Hence we operate in a very narrow viscosity range when increasing the active material mass loading of the cathode electrodes.

In order to investigate the influence of different calendering forces, the cathode electrode tapes were compressed at 17 kg cm^{-1}, 47 kg cm^{-1} and 70 kg cm^{-1}. In Fig. 6 the SEM images of these electrodes after roll-pressing and drying are depicted. In general all the electrodes show a homogenous distribution of active material particles. The SEM image of the un-pressed electrode (Fig. 6a) shows very clearly the formation of extensive cracks throughout the electrode surface due to the large shrinkage of the CMC binder during the drying procedure. This is clearly due to the high average mass loading (about 7.5 mg cm^{-2}) and the limited capability of our lab-scale equipment to properly mix and coat slurries with higher viscosity. Interestingly, however, the fissures diminish in size with increasing calendering force as can be seen in Fig. 6b–d. A closer examination of the most compressed electrode (Fig. 6d) evidence that all cracks have been closed in consequence of the applied force. Moreover the electrode surface pressed by 70 kg cm^{-1} is well flattened in comparison to the un-pressed electrode (Fig. 6a). Summarizing, strong calendering has a considerably beneficial effect on the morphology of high mass loading CMC-based NMC cathodes. Table 3 reports the electrode density of the compressed electrodes as well as their thickness reduction (in % of the original thickness).

With the purpose of investigating the effect of calendering on the electrochemical behaviour of NMC cathodes cycling tests were performed on electrodes pressed at different line force loads. The results are illustrated in Fig. 7a showing the cycling performance at 1 C rate for these electrodes. For all the tested samples the specific discharge capacity drops, as expected, to values between 130 mAh g^{-1} and 135 mAh g^{-1} after the initial 3 formation cycles at 0.1 C rate, during which capacities higher than 150 mAh g^{-1} were detected. Upon cycling at 1 C rate the un-pressed electrodes show a significantly higher capacity fading over the illustrated 70 cycles than the pressed electrodes. The differences in specific discharge capacity of the pressed electrodes are usually ranging around 1–2 mAh g^{-1}. It can, therefore, be considered that the compression step is needed to improve the long-term cyclability, however, independently from the line force load applied during the compression step all electrodes show the same behaviour upon cycling. Nevertheless, the electrode compressed at 70 kg cm^{-1} certainly showed the flatter surface and, for such a reason, is preferable.

According to the presented charge/discharge results, Fig. 7b illustrates a few, selected voltage profiles of the 70 kg cm^{-1} pressed electrode. The sloping Li-insertion plateau typically observed for NMC [43], is observed between the cut-off potentials of 3.0 V and 4.3 V. Focussing on the curves recorded at a discharge rate of 1 C, a very limited decrease of delivered capacity is noticed, corresponding to a total capacity fading of approximately 5.2% between the 4th and the 70th cycle.

Considering their promising cycling performance and superior morphological appearance, the electrodes pressed at 70 kg cm^{-1} were selected for the realization of the lithium-ion cells.

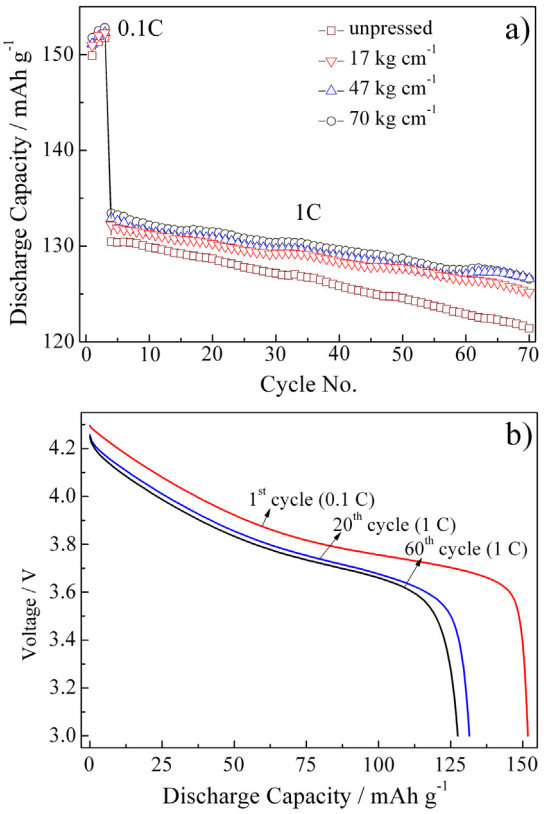

Fig. 7. Cycling performance (a) of cathode electrodes calendered at different pressures and selected voltage profiles (b) of the calendered cathode electrode (line force load: 70 kg cm^{-1}). Counter and reference electrodes: Li.

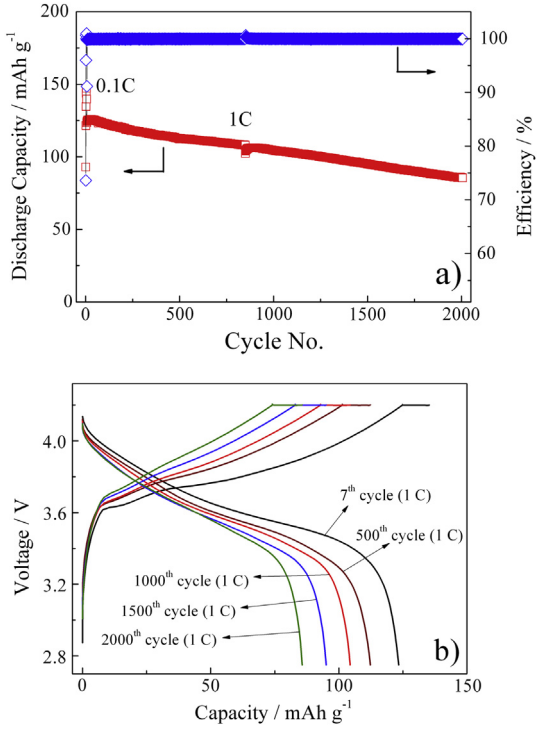

Fig. 8. Specific capacity and efficiency (a) and selected voltage profiles (b) of a full Li-ion cell comprising a high mass loading NMC cathode electrode (7.64 mg cm^{-2}, calendered at 70 kg cm^{-1}) and a SLP 30 anode electrode (3.14 mg cm^{-2}, calendered at 3 kg cm^{-1}).

3.4. Li-ion cell

The full cell electrodes were balanced, using their practical capacities at 0.1C rate, to a cathode/anode capacity ratio ranging from 1 to 1.24 to 1 to 1.34. Fig. 8a displays the cycling performance of a lithium-ion cell with the cathode mass loading of 7.64 mg cm^{-2}. After the first 1000 cycles at 1 C rate, the completely CMC-based, high mass loading cell still reached a specific capacity of 104.3 mAh g^{-1}-NMC, which corresponds to a remarkable capacity retention of almost 84% and, therefore, an average coulombic efficiency higher than 99.95%. In the course of the second 1000 cycles at a 1 C rate, the full-cell reached the end of life criteria for usage in automotive applications [10,44] (delivered capacity lower than 80% of the initial capacity) after 1293 cycles. Nevertheless, a specific capacity of 85.38 mAh g^{-1}-NMC was still delivered after 2000 cycles, which corresponds to a capacity retention of almost 70%. In Fig. 8b are depicted a few, selected voltage profiles of the lithium-ion cell at a current density corresponding to 1C. The slightly increasing polarization of the electrodes and the moderate shortening of the sloping Li-insertion (into NMC) plateau upon cycling result in the very modest capacity fading of the cell, particularly in-between the 1000th and 2000th cycle. Nonetheless, the full lithium-ion cell reached coulombic efficiencies during the overall 2000 cycles of 99.96%. Certainly these values are quite exceptional for an entirely aqueous processed Li-ion battery on a lab-scale level.

4. Conclusion

It has been proven that CMC binder is thermally stable up to 200 °C and exhibits an excellent electrochemical stability in the potential range from 0.02 V to 5.00 V. CMC was shown as a viable aqueous binder to realize NMC- as well as graphite-based electrodes with capacity loading around 10 mAh cm^{-2}. The aluminium corrosion occurring upon the cathode slurry coating was avoided by the use of a thin carbon layer. The effect of compressing such CMC-based cathode (NMC) and anode (SLP 30) electrodes was investigated. Compression of the anode electrodes did not show any substantial improvement in cycling performance, but strongly improved the surface flatness. However, high calendering forces seem to adversely affect the cycling stability. Nevertheless, the thickness of anode electrode pressed by 3.0 kg cm^{-1} was reduced from 57 μm to 53 μm and no influence on cyclic performance could be observed. On the contrary compressing the cathode electrodes proved to have a clearly beneficial effect on the cycling performance. This was especially true when considering the impact of calendering to the surface morphology of these electrodes.

All these factors led to a superior cycling performance (average efficiencies for 2000 cycles of 99.96%; capacity retention after 1000 cycles: almost 84%; capacity retention after 2000 cycles: almost 70%) of completely CMC-based, Li-ion cells with high cathode mass loading which has, to the best of our knowledge, never been shown before for aqueous processed NMC/graphite full-cells.

Acknowledgements

The authors thank the European Commission within the FP7 Projects GREENLION (Grant agreement no. 285268) for the financial support. TIMCAL is kindly acknowledged for supplying SLP 30 graphite, C-NERGY Li-Quid 101 carbon coating and C-NERGY Super C45 carbon additive.

References

[1] M.R. Palacin, Chem. Soc. Rev. 38 (2009) 2565–2575.
[2] M. Winter, R.J. Brodd, Chem. Rev. 104 (2004) 4245–4270.
[3] D. Guy, B. Lestriez, D. Guyomard, Adv. Mater. 16 (2004) 553–557.
[4] J.-S. Bridel, T. Azaïs, M. Morcrette, J.-M. Tarascon, D. Larcher, J. Electrochem. Soc. 158 (2011) A750–A759.
[5] Y.-S. He, Z.-F. Ma, X.-Z. Liao, Y. Jiang, J. Power Sources 163 (2007) 1053–1058.
[6] D. Aurbach, J. Power Sources 89 (2000) 206–218.
[7] J. Li, R.B. Lewis, J.R. Dahn, ECS Solid State Lett. 10 (2007) A17–A20.
[8] B. Scrosati, J. Garche, J. Power Sources 195 (2010) 2419–2430.
[9] M. Wachtler, M. Winter, J.O. Besenhard, J. Power Sources 105 (2002) 151–160.
[10] J. Vetter, P. Novák, M.R. Wagner, C. Veit, K.C. Möller, J.O. Besenhard, M. Winter, M. Wohlfahrt-Mehrens, C. Vogler, A. Hammouche, J. Power Sources 147 (2005) 269–281.
[11] J. Li, C. Daniel, D. Wood, J. Power Sources 196 (2011) 2452–2460.
[12] G.T. Kim, S.S. Jeong, M. Joost, E. Rocca, M. Winter, S. Passerini, A. Balducci, J. Power Sources 196 (2011) 2187–2194.
[13] A. Moretti, G.-T. Kim, D. Bresser, K. Renger, E. Paillard, R. Marassi, M. Winter, S. Passerini, J. Power Sources 221 (2013) 419–426.
[14] A. Guerfi, M. Kaneko, M. Petitclerc, M. Mori, K. Zaghib, J. Power Sources 163 (2007) 1047–1052.
[15] J.-H. Lee, J.-S. Kim, Y.C. Kim, D.S. Zang, Y.-M. Choi, W.I. Park, U. Paik, ECS Solid State Lett. 11 (2008) A175–A178.
[16] H. Buqa, M. Holzapfel, F. Krumeich, C. Veit, P. Novák, J. Power Sources 161 (2006) 617–622.
[17] C.-C. Li, Y.-W. Wang, J. Power Sources 227 (2013) 204–210.
[18] F.M. Courtel, S. Niketic, D. Duguay, Y. Abu-Lebdeh, I.J. Davidson, J. Power Sources 196 (2011) 2128–2134.
[19] J. Li, B.L. Armstrong, J. Kiggans, C. Daniel, D.L. Wood, Langmuir 28 (2012) 3783–3790.
[20] I. Kovalenko, B. Zdyrko, A. Magasinski, B. Hertzberg, Z. Milicev, R. Burtovyy, I. Luzinov, G. Yushin, Science 334 (2011) 75–79.
[21] S.S. Jeong, N. Böckenfeld, A. Balducci, M. Winter, S. Passerini, J. Power Sources 199 (2012) 331–335.
[22] L. Xie, L. Zhao, J.-l. Wan, Z.-q. Shao, F.-j. Wang, S.-y. Lv, J. Electrochem. Soc. 159 (2012) A499–A505.
[23] J. Xu, S.-L. Chou, Q.-f. Gu, H.-K. Liu, S.-X. Dou, J. Power Sources 225 (2013) 172–178.
[24] J.-H. Lee, U. Paik, V.A. Hackley, Y.-M. Choi, J. Electrochem. Soc. 152 (2005) A1763–A1769.
[25] J.-H. Lee, S. Lee, U. Paik, Y.-M. Choi, J. Power Sources 147 (2005) 249–255.
[26] W. Porcher, B. Lestriez, S. Jouanneau, D. Guyomard, J. Electrochem. Soc. 156 (2009) A133–A144.
[27] S.F. Lux, F. Schappacher, A. Balducci, S. Passerini, M. Winter, J. Electrochem. Soc. 157 (2010) A320–A325.
[28] I. Doberdo, N. Loeffler, N. Laszczynski, D. Cericola, N. Penazzi, S. Bodoardo, G.T. Kim, S. Passerini, J. Power Sources (2013) in press.
[29] M.J. Zohuriaan, F. Shokrolahi, Polym. Test. 23 (2004) 575–579.
[30] S.F. El-Kalyoubi, N.A. El-Shinnawy, J. Appl. Polym. Sci. 30 (1985) 4793–4799.
[31] D. Aurbach, M. Daroux, P. Faguy, E. Yeager, J. Electroanal. Chem. 297 (1991) 225–244.
[32] X. Zhang, R. Kostecki, T.J. Richardson, J.K. Pugh, P.N. Ross, J. Electrochem. Soc. 148 (2001) A1341–A1345.
[33] M. Morita, T. Shibata, N. Yoshimoto, M. Ishikawa, Electrochim. Acta 47 (2002) 2787–2793.
[34] X. Zhang, T.M. Devine, J. Electrochem. Soc. 153 (2006) B344–B351.
[35] E. Ligneel, B. Lestriez, A. Hudhomme, D. Guyomard, J. Electrochem. Soc. 154 (2007) A235–A241.
[36] D. Liu, Y. Wang, Y. Xie, L. He, J. Chen, K. Wu, R. Xu, Y. Gao, J. Power Sources 232 (2013) 29–33.
[37] P.C. Wang, H.P. Ding, T. Bark, C.H. Chen, Electrochim. Acta 52 (2007) 6650–6655.
[38] J. Zheng, J. Xiao, W. Xu, X. Chen, M. Gu, X. Li, J.-G. Zhang, J. Power Sources 227 (2013) 211–217.
[39] W. Rüdorff, U. Hofmann, Z. Anorg. Allg. Chem. 238 (1938) 1–50.
[40] M. Winter, J.O. Besenhard, M.E. Spahr, P. Novák, Adv. Mater. 10 (1998) 725–763.
[41] K.A. Striebel, A. Sierra, J. Shim, C.W. Wang, A.M. Sastry, J. Power Sources 134 (2004) 241–251.
[42] K. Ishii, R. Ozaki, K. Kaneko, H. Fukushima, M. Masuda, Corros. Sci. 49 (2007) 2581–2601.
[43] M.S. Whittingham, Chem. Rev. 104 (2004) 4271–4302.
[44] S. Krueger, R. Kloepsch, J. Li, S. Nowak, S. Passerini, M. Winter, J. Electrochem. Soc. 160 (2013) A542–A548.